Non-equilibrium quantum domain reconfiguration dynamics in a two-dimensional electronic crystal: experiments and quantum simulations

Jaka Vodeb*[1,2,3], Michele Diego[1], Yevhenii Vaskivskyi[1], Leonard Logaric[1], Yaroslav Gerasimenko[1], Viktor Kabanov[1], Benjamin Lipovsek[4], Marko Topic[4] and Dragan Mihailovic*[1,2,5]

[1]*Jozef Stefan Institute, Jamova 39, 1000 Ljubljana, Slovenia*

[2]*Faculty of Mathematics and Physics, University of Ljubljana, Jadranska 19, Ljubljana, Slovenia*

[3]*Institute for Advanced Simulation, Jülich Supercomputing Centre, Forschungszentrum Jülich, Wilhelm-Johnen-Straße, 52425 Jülich, Germany*

[4]*Faculty for Electrical Engineering, University of Ljubljana, Tržaška 25, 1000 Ljubljana, Slovenia*

[5]*CENN Nanocenter, Jamova 39, 1000 Ljubljana, Slovenia*

*jaka.vodeb@ijs.si, *dragan.mihailovic@ijs.si

Relaxation dynamics of complex many-body quantum systems brought out of equilibrium and subsequently trapped into metastable states is a very active field of research from both the theoretical and experimental point of view with implications in a wide array of topics from macroscopic quantum tunnelling and nucleosynthesis to non-equilibrium superconductivity and new energy-efficient memory devices. Understanding the dynamics of such systems is crucial for exploring fundamental aspects of many-body non-equilibrium quantum physics. In this work we investigate quantum domain reconfiguration dynamics in the electronic superlattice of a quantum material where classical dynamics is topologically constrained. The crossover from temperature to quantum fluctuation dominated dynamics in the context of environmental noise is investigated by directly observing charge reconfiguration with time-resolved scanning tunneling microscopy. The process is modelled using a programmable superconducting quantum simulator in which qubit interconnections correspond directly to the microscopic interactions between electrons in the quantum material. Crucially, the dynamics of both the experiment on the quantum material and the simulation is driven by spectrally similar pink noise. We find that the simulations reproduce the emergent time evolution and temperature dependence of the experimentally observed electronic domain dynamics remarkably well. The combined experiment and simulations lead to a better understanding of noise-driven quantum dynamics in open quantum systems. From a practical viewpoint, the results are important for understanding the origin of the retention time in non-volatile memory devices such as those based on 1T-TaS_2.

Introduction

Many-body systems emerging through symmetry-breaking phase transitions often end up in inhomogeneous intermediate states before reaching a homogeneous ground state. In the aftermath of second-order transitions, such as the superconducting transition in type-2 superconductors, fluctuations in the phase of the order parameter force causally unconnected regions to evolve independently, forming mesoscopic vortex structures[1–3]. In the aftermath of first-order phase transitions, the classical dynamics involves nucleation of the new phase, followed by coalescence[4] and "ripening"[5]. Topological and jamming transitions present more complex non-equilibrium dynamics that recently became topics of wider interest[6,7]. In classical systems, the kinetics is primarily diffusion-driven, while metastability arises from symmetry or topological constraints. In quantum systems[8], particularly at low temperatures we may expect to observe either coherent quantum dynamics for perfectly isolated systems, or incoherent macroscopic tunneling (IMT) aided by noise-assisted processes causing transitions between different mesoscopic state configurations[9].

The challenge is to quantitatively measure state reconfigurations of a many-body system in order to identify mesoscopic tunneling processes between different domain configurations, and then compare such data with model simulations of the dynamics. Because such processes are quite common, and have important potential applications[10], the ability to faithfully simulate their dynamics on a quantum level would lead to significant progress in understanding metastable states in quantum materials and non-equilibrium quantum devices. In electronic crystals, the ordering of domains and discommensurations are traditionally modelled classically by an anisotropic Ising model with competing interactions[11] or by continuum models[12,13], but these models give little insight into how inhomogeneities evolve in the quantum regime. Ab-initio methods can give detailed electronic band structure information of individual domain walls[14], but cannot be used to simulate the emergent many-body collective dynamics. Non-equilibrium dynamics pose an especially difficult challenge to faithful classical simulation[15], where an exponentially large Hilbert space dimension is required. Brute force state vector simulations can barely exceed 50 qubits even on the best high-performance computer clusters currently available[16]. On the other hand, quantum Monte Carlo calculations with added noise are not developed for direct probing of non-equilibrium dynamics, and it is still an open question whether, and how they could be applied at all. Quantum simulations of ground state properties in many body systems, as well as metastable decay of complex systems using ultracold atomic lattices have recently been demonstrated[17,18], and a lot of recent attention has focused on noisy intermediate scale quantum (NISQ) processors. But extension to real-world non-equilibrium systems requiring thousands

of qubits in 2D, such as is addressed here, is particularly challenging because it requires extreme, currently unavailable computational resources, as well as presently still unachievable control of decoherence.

Macroscopic quantum motion of domain walls in the presence of noise has attracted a lot of attention since the 1980s. Typically, spin tunnelling in a ferromagnets[19,20] is considered, which may be formulated in terms of domain wall tunnelling[21,22]. Research of this type includes magnetotransport measurements on thin ferromagnetic wires[23], and magnetization experiments on single particles[24,25], nanomagnet ensembles[26–28] and rare-earth multilayers[29]. A second method is to investigate macroscopic disordered ferromagnets[30–33]. Here we report for the first time a study of quantum noise driven domain wall dynamics of strongly correlated electrons. Our experimental system is the prototype quasi-two-dimensional (2D) strongly correlated transition metal dichalcogenide material 1T-TaS_2[34]: It is chosen because it displays prototypical electronic crystal ordering behavior[35]. As a result of the strong electron-phonon interaction in this material, the electronic kinetic energy K is exponentially reduced[36], and Coulomb energy V becomes dominant[37]. The essential physics in this regime thus comes from the formation of mutually repulsive heavily dressed quasiparticles – polarons[35], with a variety of polaron-ordered states and metastable domain structures[35,38,39]. In response to external perturbation 1T-TaS_2 exhibits fundamentally interesting and practically useful switching behavior[10,35,40–42] between different metastable states associated with different configurations of domains of the low-temperature electronic superlattice. At low temperatures, the temporal reconfigurations can be effectively investigated by scanning tunneling microscopy (STM). The classical many-body relaxation dynamics of such domain states is topologically inhibited[43,44], effectively creating an energy barrier for the transition between different domain configurations. In such a system where the dynamics of classical processes is topologically inhibited, quantum dynamics is necessary for metastable state relaxation, especially at low temperatures. Understanding these processes is directly relevant for controlling functional properties, and in particular data retention in non-volatile configuration memory devices[10,45].

Using a new approach to modeling emergent non-equilibrium behavior, we investigate the electronic domain dynamics in 1T-TaS_2, with a parallel simulation using a superconducting quantum simulator. The decoherence of domains in the simulation – just as in 1T-TaS_2 – is governed by $1/\nu$ pink noise[46,47], so the simulations can be thought to utilize the principles of simulating nature with nature, as originally proposed by Feynman[48]. Here we find that the quantum simulator describes the natural noise-driven processes remarkably well. The reproduction of the emergent metastable decay

behavior that is observed in the experiments is particularly striking. The results lead to valuable insights into how microscopic many-body interactions between electrons on a superlattice conspire to display metastable quantum domain relaxation dynamics observed in the experiments on 1T-TaS_2.

Results

Domain Reconfiguration Measurements in 1T-TaS_2. In our experiments, a metastable domain state in the $\sqrt{13} \times \sqrt{13}$ electronic superlattice of 1T-TaS_2 is set up by electrical pulse charge injection through an STM tip[43,49,50] (Fig. 1c). As the domain structure evolves in time, its configuration is recorded periodically by STM at different temperatures. A relaxation sequence at 5 K is shown in Fig.1c. The tip is retracted and set to zero bias between measurements to avoid reconfiguration by spurious signals from the tip. This measurement results in classical sequential "snapshots" of the domain configurations at different temperatures (see SI for experimental details). The reconfigurations between sequential images are quantified by measuring the Hamming distance, defined here as the number of altered occupied polaron positions between frames (Fig.1c), and expressed as the fraction of polarons moved $f = \Delta N/N$, where N is the total number of polarons per frame (Fig.1d). Characteristically, jumps of f appear in time (Fig.1d), reflecting the discrete nature of the domain reconfiguration process[51]. When f is averaged over a large number of scans on different areas of the sample an approximately exponential decay of is observed (Fig. 1e). The classical power law time dependencies $f(t) \sim r(t)^2 \sim t^{-1}$ or $t^{-2/3}$, that would be characteristic of nucleation and coalescence processes[4] respectively at higher temperatures[52], cannot be made to fit the 5 K domain relaxation data (Fig.1e). Considering the difference of the processes involved, this is not surprising.

A crucial test of the experiments is to see if, and how, the STM tip influences the reconfiguration process. Comparing $f(t)$ obtained by tip scanning at regular intervals (Fig.1e), with $f(t)$ measured under identical experimental conditions, but with a retracted tip over a longer time interval, we see in Fig.1f that the two relaxation times are very similar: $\tau = 1040 \pm 90\ s$ and $945 \pm 80\ s$ respectively, implying that within experimental error the influence of the STM tip is negligible. A number of other tests that support this conclusion are given in the supplement, including a detailed calculation of Joule heating by the STM tip current. We have thus established that the noise in 1T-TaS_2 does not originate from the STM tip, but has a different non-thermal origin. Other possible excitation sources are acoustic phonons, quantum fluctuations in two-level systems (TLSs) in the sample, the substrate and at the interface, as well as spurious external electro-magnetic fields brought by the grounded sample contact. Importantly for our purposes, in 1T-TaS_2 the noise has been experimentally shown to have a $\sim 1/\nu$, frequency dependence.[46]

The dependence of the reconfiguration rate $R(T) = \frac{1}{\Delta t}\int_0^{t_{exp}} f(t)dt$, where Δt is the time interval between subsequent image samplings and t_{exp} the duration of the experiment at temperature T, on sample temperature in 1T-TaS_2 is shown in Fig. 1g for $\Delta t \cong 480\ s$. $R(T)$ exhibits a distinct crossover

from T-independent to T-dependent behavior at a temperature $T_0 \approx 20\ K$. The data can be fit well to: $R(T) = R_q + R_0 \exp(-E_M/k_B T)$, where $R_q \simeq 8 \pm 1 \times 10^{-4}\ s^{-1}$ is the T-independent tunneling rate, and the second term describes T-activated hopping across a barrier. The value $E_M = 6 \pm 3\ meV$ obtained from the fit to the data in Fig. 1g is not far from the activation energy $E_A = 10 \sim 20\ meV$ obtained from previous macroscopic resistance relaxation measurements of bulk samples[51], providing an important experimental consistency check.

Since by STM we observe "snapshots", which are effectively separated by large time windows, we assume that reconfigurations correspond to single escape events from a local minimum in a multidimensional free energy landscape of dimension $D = 2^N$, where N is the number of atomic sites, shown schematically in 1D as a function f is in the insert to Fig.1d. Different minima in $E(f)$ correspond to different configurational states, while the excited states within the wells correspond to configuration processes which conserve f, such as translations.

Quantum decay rate. First we check whether existing analytical theory of noise mediated quantum dynamics in the presence of a thermal bath can explain the crossover in $R(T)$. The canonical Kramers-Caldeira-Legget (KCL) quantum decay rate (QDR) theory[53,54] assumes a system moving through a cubic potential in a 1D configurational landscape (Fig. 2b) and does indeed predict an $R(T)$ crossover. Here, we approximate the movement of polarons in 1T-TaS_2 through its multidimensional energy landscape with a series of local 1D paths, each representing a single reconfiguration event (see insert to Fig. 1d). According to KCL, polarons in 1T-TaS_2 are initially trapped in the metastable minimum of the cubic potential separated by a barrier from a lower energy state, which can be overcome by either noise mediated incoherent quantum tunneling at low T or thermal activation at high T. The crossover occurs at temperature T_0 within a range ΔT. If we take the experimental values E_M, $T_0 = 20\ K$ and $\Delta T = 10\ K$, obtained from Fig. 1g and plug them into KCL theory in order to characterize an average reconfiguration event, it predicts $\frac{E_M}{\hbar\omega_0} \simeq 0.4 \sim 1.4$, where $\hbar\omega_0$ is the kinetic energy scale of polarons in 1T-TaS_2. This is in direct contradiction with the underlying assumptions of KCL theory $\left(\frac{E_M}{\hbar\omega_0} \gg 1\right)$. Therefore, the assumptions of the KCL theory are fundamentally incompatible with the observed behavior in 1T-TaS_2. An extension of the KCL theory into the multidimensional case as well as $E_M \sim \hbar\omega_0$ is required, which unfortunately currently does not exist.

Quantum simulation of domain reconfiguration dynamics. An alternative to analytical theory is simulation of the system microscopically, and examine the emergent behavior in comparison with experiments of the dynamics of domains in 1T-TaS_2. We start with a single Ta band of tight-binding

electrons[55] coupled to phonons via the Fröhlich interaction, interacting via a long-range Coulomb repulsion $V_c(i,j)$. In the limit of strong electron-phonon interaction, such a model exhibits repulsive polarons as slow quasiparticles with an exponentially suppressed tunneling matrix element t_{ij}[36]. Here we focus on charge ordering of such polarons and neglect the spin degree of freedom, attributing to each atomic site a binary variable $q_i \in \{0,1\}$ (a qubit), which represents the polaron occupancy of site i on a triangular lattice and assume only nearest neighbor repulsion $V(i,j)$. The Hamiltonian is then $H_M = -\sum_{\langle ij \rangle} t_{ij} c_i^\dagger c_j + \sum_{\langle ij \rangle} V(i,j) q_i q_j - \mu \sum_i q_i$, with $c_i^\dagger c_i = q_i$, and chemical potential is μ, which is chosen such that the ground state at $t_{ij} = 0$ is a triangular polaronic superlattice where each polaron can occupy one of 3 atomic lattice sites (Fig. 2a).

Quantum dynamics calculations of sufficient system sizes required to capture reconfiguration dynamics of hundreds of polarons in the experiment are presently unrealistic on a classical digital computer. We thus explore the alternative possibility of using a programmable quantum annealer D-wave Advantage 6.1 (PQA) to model the dynamics, which has already been shown to exhibit multiqubit tunnelling in the presence of a thermal noise[56–59]. Importantly, the superconducting qubit TLS dynamics of the PQA is mediated by coupling to TLSs in the environment which has a very similar $1/\nu$ frequency dependence of the noise as 1T-TaS_2[46,47]. (A more detailed comparison of noise characteristics is made in the SI.) The PQA is designed for simulations that are extensions of the transverse field Ising model (TFIM) with adjustable temperature:

$$H_{PQA}/k_B T = \left(-\sum_i \sigma_i^x /2 + r[s(t)] \left(\sum_{\langle ij \rangle} V(i,j) q_i q_j - \mu \sum_i q_i \right) \right) / T_{eff}[s(t)],$$

where $\sigma_i^z = 2q_i - 1$, $\sigma_i^{x,z}$ are Pauli matrices operating on q_i and $s(t)$ is a custom time dependent function ranging from 0 to 1, conventionally called the annealing schedule in the simulation. The TFIM model was originally introduced to describe collective motion between of protons in microscopic hydrogen bonded double well potentials[60]. It is known that solutions of the TFIM in 1D can be used to model domain walls propagating as free particles in the background of strong interactions with an associated false vacuum state that describes the transitions between different domain configurations[61]. It has also been shown recently[62] that with a 2D TFIM with strong nearest neighbor interactions, domain walls behave as free fermions with conventional hopping $\sum_{\langle ij \rangle} c_i^\dagger c_j + h.c.$ in the limit of strong interactions ($r \gg 1$), which is closely analogous to domain walls between polaronic lattices. Through $s(t)$ we are able to control the two tunable parameters in our simulation: the effective dimensionless temperature $T_{eff}[s(t)]$ and the ratio between the potential and kinetic energy, $r[s(t)]$[63]. We map μ onto individual qubits biases and $V(i,j)$ to couplers between qubits, with a 4/3 ratio of physical to

logical qubits (Fig. 2b). In this way, the TFIM makes it possible to describe the tunneling dynamics between different 2D domain states of 1T-TaS_2.

The calculation should be considered as a salient model which ignores coupling to phonons, as well as long-range interactions, but given that the classical charged lattice gas modelling describes low-temperature ordering in 1T-TaS_2[38], the use of the TFIM in the limit of strong interaction may be justified for weak quantum tunneling effects at low T. The simulation does not explicitly address the sources of environmental noise[64], but it is assumed to have $1/\nu$ frequency dependence, similar as in 1T-TaS_2[46], based on previous measurements of the PQA[47]. (More discussions on the application of the TFIM model on the D-Wave Advantage quantum annealer is given in the SI.).

We emulate the STM measuring process by initializing the system of qubits (polarons) into a domain state (as a product state in the qubit q_i basis) similar to the initially observed states in 1T-TaS_2. The domain walls separate the 3 possible ground states. (For simplicity, in the simulation we have used 3 rather than 13 possible degenerate ground states, as in 1T-TaS_2). The PQA allows us to adiabatically tune $r[s(t)]$ and $T_{eff}[s(t)]$ via $s(t)$ in order to bring them to the range of values for which we want to observe dynamics. After we let the system of qubits evolve for a preset amount of time, we perform a measurement and observe the polaronic configuration that the qubits have evolved into. Then, we use the measured configuration as the new initial product state, thereby faithfully emulating the iterative STM measurement. From the point of view of Hamiltonians, we start with $H_{PQA}(t=0) = \left(-\sum_i \sigma_i^x + r[1]\left(\sum_{\langle ij\rangle} V(i,j) q_i q_j - \mu \sum_i q_i\right)\right)/T_{eff}[1]$, where $r[1] \approx 10^{10}$, and initialize the qubits into the initial domain state in the qubit computational basis, then adiabatically tune to $H_{PQA}\left(t=\frac{t_a}{2}\right) = \left(-\sum_i \sigma_i^x/2 + r\left[s\left(\frac{t_a}{2}\right)\right]\left(\sum_{\langle ij\rangle} V(i,j) q_i q_j - \mu \sum_i q_i\right)\right)/T_{eff}\left[s\left(\frac{t_a}{2}\right)\right]$ and let the system evolve in time, and finally adiabatically tune back to $H_{PQA}(t=t_a) = H_{PQA}(t=0)$, which constitutes a measurement. The annealing time t_a is of the order of 10 μs and the energy scale of H_{PQA} is a few GHz. We focus on values $r\left[s\left(\frac{t_a}{2}\right)\right] \gg 1$, where the kinetic energy of domain walls is small compared to the interaction energy and study the behavior of domain wall dynamics at different T_{eff}. Details on the methodology are given in the SI.

We observe translations and melting of the domain walls towards one of the 3 uniform ground states from the initial domain wall state, just as it occurs in 1T-TaS_2 (Fig. 1c and Fig. 2c). The characteristics of the domain melting processes captured by the fraction of moved polarons $f(t)$ in 1T-TaS_2 (Fig. 1d) also experiences intermediate saturations and jumps in the PQA (Fig. 2d). Most

importantly, both systems exhibit a crossover in the relaxation rate $R(T_{eff})$ from T-dependent activation processes at high T to T-independent noise mediated quantum tunnelling events at low T (Fig. 1g and Fig. 2e). $R(T_{eff})$ saturates to a T-independent non-zero rate due to slow system dynamics compared to the sampling time, which is the rate at which we measure with the STM tip in 1T-TaS_2 or the rate of qubit measurements in the PQA. If the system is given enough time to fully relax to the uniform ground state, then the dynamics eventually stops. In order to reproduce the experimental timescale of the dynamics ($\sim 1000\ s$), we need to set $r \approx 58$.As an indirect comparison, the usual criterion for Wigner crystallization in 2D $r_s = \frac{e^2 m^*}{\hbar^2 \sqrt{n}} = 31{\sim}38$[34,65], justifying the use of a dominant interaction term with small kinetic energy in the calculations.

Discussion

Let us interpret the physical processes involved in noise mediated quantum tunnelling. 1T-TaS_2 and the PQA are both described by a Hamiltonian H_S, coupled via H_I to an external thermal bath B with a $1/\nu$ noise spectrum at temperature T, where the total Hamiltonian is $H = H_S + H_I + H_B$. We can represent an arbitrary bath described by a spectral function $\Im(\omega) = \frac{\pi}{2}\sum_\alpha (C_\alpha^2/m_\alpha\omega_\alpha)\delta(\omega - \omega_\alpha)$ with a system of decoupled harmonic oscillators (HOs) with mass m_α, frequencies ω_α, and couplings C_α in H_I[9]. Temperature effects are taken into account by populating each HO with a Bose-Einstein distribution with temperature T, meaning that at low T HOs effectively reduce to TLSs. In the limit of $H_I \to 0$ we would only observe pure tunnelling events from an initial classical polaronic configuration into other configurations, determined by their overlap with instantaneous eigenstates during the adiabatic evolution, as well as the shape of the annealing schedule. By bringing the initial classical configuration adiabatically into a superposition state of multiple configurations and then back, we introduce a probability of tunnelling to other configurations involved in the superpositions. We found that the kinetic energy contribution is very small compared to the interaction ($r \approx 58$), which means that pure tunnelling events would be highly constrained in the energy difference between the initial and final configuration. If fact, the energy difference tends to 0 in the limit of $r \to \infty$, meaning that we would have no configurational changes at $T = 0$ and zero noise.

Now we discuss the effect of noise and temperature on quantum tunnelling. The number of HOs, populated at temperature T, required to describe a particular spectral function is much larger than the number of polarons, meaning that they effectively serve as an infinite energy reservoir for the polarons and are constantly bringing them into thermal equilibrium with respect to T. Noise is represented by the influence of HOs on the energy spectrum of H_S, which is a static energy shift of energy levels[64].

The simplest example is when both H_B and H_S are two-level systems. The two levels of H_S represent two polaronic eigenstates and the two levels of H_B are the first two HO levels. Each polaronic state is split by $\hbar\omega_\alpha$ into two levels by adding the HO degree of freedom, meaning that a properly chosen ω_α can bring two polaronic states to the same energy, thereby making quantum tunnelling between them possible. This is what we mean by noise mediated macroscopic quantum tunnelling. We introduce the $1/\nu$ noise spectrum by increasing the number of HOs and choosing appropriate C_α, m_α and ω_α. The polaronic state energy level then becomes an energy band with width W, given by an integral over the noise spectrum, as shown in Fig. 2f. If energy bands overlap, then a transition between the bath degrees of freedom can already induce a polaronic configurational change. If they do not overlap, the energy gap is still reduced by W, increasing the probability for a transition. Both represent incoherent macroscopic tunneling (IMT) processes.

Quantum simulation gives us some other unique insights into the emergent tunneling phenomenon. The dynamics of the two systems is governed by an anharmonic metastable state potential in terms of the configurational coordinate, measured by f, for 1T-TaS_2 and the PQA respectively. While the washboard potential and two-level system dynamics of flux qubits in the PQA emerge from the device concept, the energy landscape of the metastable state of 1T-TaS_2 is determined by the topology and the microscopic details of the domain structure arising from discommensurations[14]. The extracted parameters from the simulations describing the emergent processes are the barrier energy E_B (height) and the barrier width w which describe the rate of tunneling between domain configurations. In 1T-TaS_2, the thermal activation energy E_B is determined directly from the T-dependence of the rate in Fig. 1c or resistivity relaxation to be $E_M \simeq 10 \sim 20\ meV$. On the other hand, w is related to f, where both are measured in terms of the configurational coordinate, which is set by the state of N Bloch spheres representing qubits, parametrized by $2N$ spherical angles. The plot of $f(t)$ in Fig. 1d thus reflects the tunnel barrier width for each measured reconfiguration step.

Conclusion

The motivation for the present quantum treatment arose from the fact that temperature-independent electronic domain relaxation in 1T-TaS_2 at low temperatures cannot be explained by classical processes because their relaxation is topologically inhibited[42]. Yet we find that the phenomenological parameters extracted from the T-dependence of the relaxation rate and the crossover to T-dependent dynamics are inconsistent with conventional quantum decay. Introducing a new approach for modelling the domain dynamics we use a microscopic model implemented on a superconducting qubit processor, directly mapping the electron-electron interactions onto the PQA inter-qubit connections. In the crucial next

step which we demonstrate here is to treat the noise from the surroundings as coupled two-level systems (HOs) with the ubiquitous $1/\nu$ frequency dependence that has been shown experimentally to be present in both 1T-TaS_2[46] and the PQA[47]. The emergent many-body dynamics and associated domain reconfigurations are thus simulated solely on the basis of microscopic interactions with a single adjustable parameter r tuning the 'quantum-ness' of the system. The simulations clearly display the crossover from T-activated dynamics to T-independent domain melting that is experimentally observed in the STM measurements, giving direct insight into how the phenomenological relaxation rates emerge from microscopic interactions. The present calculations demonstrate the usefulness of simulations on a noisy quantum processor for modelling emergent non-equilibrium many-body dynamics. With appropriate mapping, such an approach can be applied to other non-equilibrium open quantum systems that are subject to external sources of incoherent noise - including quantum materials such as the quantum paraelectric $SrTiO_3$[66], various hydrogen-bonded systems[67], in the folding of proteins through a similarly multidimensional, topologically defined energy landscape[68], or tunneling between false vacuum states that emerge from elementary interactions[69–71]. Apart from fundamental interest, modeling quantum reconfiguration dynamics is important for low-temperature memory devices[41], in which quantum domain melting processes functionally limit the long-term data retention[51].

References

1. Kibble, T. W. B. Topology of cosmic domains and strings. *J. Phys. Math. Gen.* **9**, 1387–1398 (1976).
2. Zurek, W. H. Cosmological experiments in superfluid helium? *Nature* **317**, 505–508 (1985).
3. Monaco, R., Mygind, J., Aaroe, M., Rivers, R. J. & Koshelets, V. P. Zurek-Kibble Mechanism for the Spontaneous Vortex Formation in Nb − Al / Al ox / Nb Josephson Tunnel Junctions: New Theory and Experiment. *Phys. Rev. Lett.* **96**, 180604 (2006).
4. Pitaevskii. *Physical Kinetics*. (Butterworth-Heinemann, 1981).
5. Baldan, A. Review Progress in Ostwald ripening theories and their applications to nickel-base superalloys Part I: Ostwald ripening theories. *J. Mater. Sci.* **37**, 2171–2202 (2002).
6. Kosterlitz, J. M. & Thouless, D. J. Ordering, metastability and phase transitions in two-dimensional systems. *J. Phys. C Solid State Phys.* **6**, 1181–1203 (1973).
7. Gerasimenko, Y. A. *et al.* Quantum jamming transition to a correlated electron glass in 1T-TaS2. *Nat. Mater.* **18**, 1078–1083 (2019).

8. Lifshitz, I. M. & Kagan, Yu. Quantum Kinetics of Phase Transitions at Temperatures Close to Absolute Zero. *Sov. Phys. JETP* **35**, (1972).
9. Leggett, A. J. *et al.* Dynamics of the dissipative two-state system. *Rev. Mod. Phys.* **59**, 1–85 (1987).
10. Mraz, A. *et al.* Charge Configuration Memory Devices: Energy Efficiency and Switching Speed. *Nano Lett.* **22**, 4814–4821 (2022).
11. Villain, J. & Bak, P. Two-dimensional ising model with competing interactions : floating phase, walls and dislocations. *J. Phys.* **42**, 657–668 (1981).
12. Villain, J. Commensurate-incommensurate transition of krypton monolayers on graphite: A low temperature theory. *Surf. Sci.* **97**, 219–242 (1980).
13. McMillan, W. L. Theory of discommensurations and the commensurate-incommensurate charge-density-wave phase transition. *Phys. Rev. B* **14**, 1496–1502 (1976).
14. Park, J. W., Lee, J. & Yeom, H. W. Zoology of domain walls in quasi-2D correlated charge density wave of 1T-TaS2. *Npj Quantum Mater.* **6**, 32 (2021).
15. Daley, A. J. *et al.* Practical quantum advantage in quantum simulation. *Nature* **607**, 667–676 (2022).
16. Arute, F. *et al.* Quantum supremacy using a programmable superconducting processor. *Nature* vol. 574 (2019).
17. Meng, Z. *et al.* Atomic Bose–Einstein condensate in twisted-bilayer optical lattices. *Nature* (2023) doi:10.1038/s41586-023-05695-4.
18. Tan, W. L. *et al.* Domain-wall confinement and dynamics in a quantum simulator. *Nat. Phys.* **17**, 742–747 (2021).
19. Chudnovsky, E. M. & Gunther, L. Quantum Tunneling of Magnetization in Small Ferromagnetic Particles. *Phys. Rev. Lett.* **60**, 661–664 (1988).
20. Kleemann, W. Universal Domain Wall Dynamics in Disordered Ferroic Materials. *Annu. Rev. Mater. Res.* **37**, 415–448 (2007).
21. Stamp, P. C. E., Chudnovsky, E. M. & Barbara, B. QUANTUM TUNNELING OF MAGNETIZATION IN SOLIDS. *Int. J. Mod. Phys. B* **06**, 1355–1473 (1992).
22. Braun, H.-B., Kyriakidis, J. & Loss, D. Macroscopic quantum tunneling of ferromagnetic domain walls. *Phys. Rev. B* **56**, 8129–8137 (1997).

23. Hong, K. & Giordano, N. Evidence for domain wall tunnelling in a quasi-one dimensional ferromagnet. *J. Phys. Condens. Matter* **8**, L301–L306 (1996).
24. Coppinger, F. *et al.* Single Domain Switching Investigated Using Telegraph Noise Spectroscopy: Possible Evidence for Macroscopic Quantum Tunneling. *Phys. Rev. Lett.* **75**, 3513–3516 (1995).
25. Wernsdorfer, W. *et al.* Macroscopic Quantum Tunneling of Magnetization of Single Ferrimagnetic Nanoparticles of Barium Ferrite. *Phys. Rev. Lett.* **79**, 4014–4017 (1997).
26. Awschalom, D. D., Smyth, J. F., Grinstein, G., DiVincenzo, D. P. & Loss, D. Macroscopic quantum tunneling in magnetic proteins. *Phys. Rev. Lett.* **68**, 3092–3095 (1992).
27. Friedman, J. R., Sarachik, M. P., Tejada, J. & Ziolo, R. Macroscopic Measurement of Resonant Magnetization Tunneling in High-Spin Molecules. *Phys. Rev. Lett.* **76**, 3830–3833 (1996).
28. Thomas, L. *et al.* Macroscopic quantum tunnelling of magnetization in a single crystal of nanomagnets. *Nature* **383**, 145–147 (1996).
29. Barbara, B. *et al.* Quantum tunnelling in magnetic particles, layers and multilayers. *Phys. Scr.* **T49A**, 268–273 (1993).
30. Uehara, M. & Barbara, B. Noncoherent quantum effects in the magnetization reversal of a chemically disordered magnet : SmCo3.5Cu1.5. *J. Phys.* **47**, 235–238 (1986).
31. Tejada, J., Zhang, X. X. & Chudnovsky, E. M. Quantum relaxation in random magnets. *Phys. Rev. B* **47**, 14977–14987 (1993).
32. Vitale, S., Cavalleri, A., Cerdonio, M., Maraner, A. & Prodi, G. A. Thermal equilibrium noise with 1/ *f* spectrum in a ferromagnetic alloy: Anomalous temperature dependence. *J. Appl. Phys.* **76**, 6332–6334 (1994).
33. Arnaudas, J. I., Del Moral, A., De La Fuente, C., Ciria, M. & De Groot, P. A. J. Mesoscopic spin tunneling in the hard-random-axis-magnet amorphous alloy Tb 2 Fe. *Phys. Rev. B* **50**, 547–550 (1994).
34. Wigner, E. On the Interaction of Electrons in Metals. *Phys. Rev.* **46**, 1002–1011 (1934).
35. Bozin, E. S. *et al.* Crystallization of polarons through charge and spin ordering transitions in 1T-TaS2. *Nat. Commun.* **14**, 7055 (2023).
36. Alexandrov, A. S. & Mott, N. F. *Polarons & bipolarons*. (World Scientific, 1995).

37. Fazekas, P. & Tosatti, E. Electrical, structural and magnetic properties of pure and doped 1T-TaS 2. *Philos. Mag. B* **39**, 229–244 (1979).
38. Vodeb, J. *et al.* Configurational electronic states in layered transition metal dichalcogenides. *New J. Phys.* **21**, 083001 (2019).
39. Ravnik, J. *et al.* A time-domain phase diagram of metastable states in a charge ordered quantum material. *Nat. Commun.* **12**, 2323 (2021).
40. Stojchevska, L. *et al.* Ultrafast switching to a stable hidden quantum state in an electronic crystal. *Science* **344**, 177–180 (2014).
41. Vaskivskyi, I. *et al.* Fast electronic resistance switching involving hidden charge density wave states. *Nat. Commun.* **7**, 11442 (2016).
42. Mraz, A. *et al.* Manipulation of fractionalized charge in the metastable topologically entangled state of a doped Wigner crystal. *Nat. Commun.* **14**, 8214 (2023).
43. Gerasimenko, Y. A., Karpov, P., Vaskivskyi, I., Brazovskii, S. & Mihailovic, D. Intertwined chiral charge orders and topological stabilization of the light-induced state of a prototypical transition metal dichalcogenide. *Npj Quantum Mater.* **4**, 32 (2019).
44. Kranjec, A. *et al.* Electronic Dislocation Dynamics in Metastable Wigner Crystal States. *Symmetry* **14**, 926 (2022).
45. Mihailovic, D. *et al.* Femtosecond data storage, processing, and search using collective excitations of a macroscopic quantum state. *Appl. Phys. Lett.* **80**, 871–873 (2002).
46. Salgado, R. *et al.* Low-frequency noise spectroscopy of charge-density-wave phase transitions in vertical quasi-2D 1T-TaS $_2$ devices. *Appl. Phys. Express* **12**, 037001 (2019).
47. Whiticar, A. M. *et al.* Probing flux and charge noise with macroscopic resonant tunneling. *Phys. Rev. B* **107**, 075412 (2023).
48. Feynman, R. P. Simulating physics with computers. *Int. J. Theor. Phys.* **21**, 467–488 (1982).
49. Ma, L. *et al.* A metallic mosaic phase and the origin of Mott-insulating state in 1T-TaS2. *Nat. Commun.* **7**, 10956 (2016).
50. Cho, D. *et al.* Nanoscale manipulation of the Mott insulating state coupled to charge order in 1T-TaS2. *Nat. Commun.* **7**, 10453 (2016).

51. Vaskivskyi, I. *et al.* Controlling the metal-to-insulator relaxation of the metastable hidden quantum state in 1T-TaS $_2$. *Sci. Adv.* **1**, e1500168 (2015).
52. Laulhé, C. *et al.* Ultrafast Formation of a Charge Density Wave State in 1 T − TaS 2 : Observation at Nanometer Scales Using Time-Resolved X-Ray Diffraction. *Phys. Rev. Lett.* **118**, 247401 (2017).
53. Hänggi, P., Talkner, P. & Borkovec, M. Reaction-rate theory: fifty years after Kramers. *Rev. Mod. Phys.* **62**, 251–341 (1990).
54. Grabert, H., Olschowski, P. & Weiss, U. Quantum decay rates for dissipative systems at finite temperatures. *Phys. Rev. B* **36**, 1931–1951 (1987).
55. Ritschel, T. *et al.* Orbital textures and charge density waves in transition metal dichalcogenides. *Nat. Phys.* **11**, 328–331 (2015).
56. Boixo, S. *et al.* Computational multiqubit tunnelling in programmable quantum annealers. *Nat. Commun.* **7**, 1–7 (2016).
57. Boixo, S. *et al.* Evidence for quantum annealing with more than one hundred qubits. *Nat. Phys.* **10**, 218–224 (2014).
58. Boixo, S., Albash, T., Spedalieri, F. M., Chancellor, N. & Lidar, D. A. Experimental signature of programmable quantum annealing. *Nat. Commun.* **4**, 1–8 (2013).
59. Denchev, V. S. *et al.* What is the computational value of finite-range tunneling? *Phys. Rev. X* **6**, 1–19 (2016).
60. De Gennes, P. G. Collective motions of hydrogen bonds. *Solid State Commun.* **1**, 132–137 (1963).
61. Lagnese, G., Surace, F. M., Kormos, M. & Calabrese, P. False vacuum decay in quantum spin chains. *Phys. Rev. B* **104**, L201106 (2021).
62. Balducci, F., Gambassi, A., Lerose, A., Scardicchio, A. & Vanoni, C. Localization and Melting of Interfaces in the Two-Dimensional Quantum Ising Model. *Phys. Rev. Lett.* **129**, 120601 (2022).
63. QPU-Specific Characteristics — D-Wave System Documentation documentation. https://docs.dwavesys.com/docs/latest/doc_physical_properties.html#doc-qpu-characteristics.
64. Amin, M. H. S., Averin, D. V. & Nesteroff, J. A. Decoherence in adiabatic quantum computation. *Phys. Rev. A* **79**, 022107 (2009).

65. Drummond, N. D. & Needs, R. J. Phase Diagram of the Low-Density Two-Dimensional Homogeneous Electron Gas. *Phys. Rev. Lett.* **102**, 126402 (2009).
66. Kustov, S., Liubimova, I. & Salje, E. K. H. Domain Dynamics in Quantum-Paraelectric SrTiO 3. *Phys. Rev. Lett.* **124**, 016801 (2020).
67. Van Voorhis, T. *et al*. The Diabatic Picture of Electron Transfer, Reaction Barriers, and Molecular Dynamics. *Annu. Rev. Phys. Chem.* **61**, 149–170 (2010).
68. Shank, E. A., Cecconi, C., Dill, J. W., Marqusee, S. & Bustamante, C. The folding cooperativity of a protein is controlled by its chain topology. *Nature* **465**, 637–640 (2010).
69. Coleman, S. Fate of the false vacuum: Semiclassical theory. *Phys. Rev. D* **15**, 2929–2936 (1977).
70. Linde, A. Inflationary Cosmology. in *Inflationary Cosmology* (eds. Lemoine, M., Martin, J. & Peter, P.) vol. 738 1–54 (Springer Berlin Heidelberg, 2008).
71. Ng, K. L., Opanchuk, B., Thenabadu, M., Reid, M. & Drummond, P. D. Fate of the False Vacuum: Finite Temperature, Entropy, and Topological Phase in Quantum Simulations of the Early Universe. *PRX Quantum* **2**, 010350 (2021).

Figures

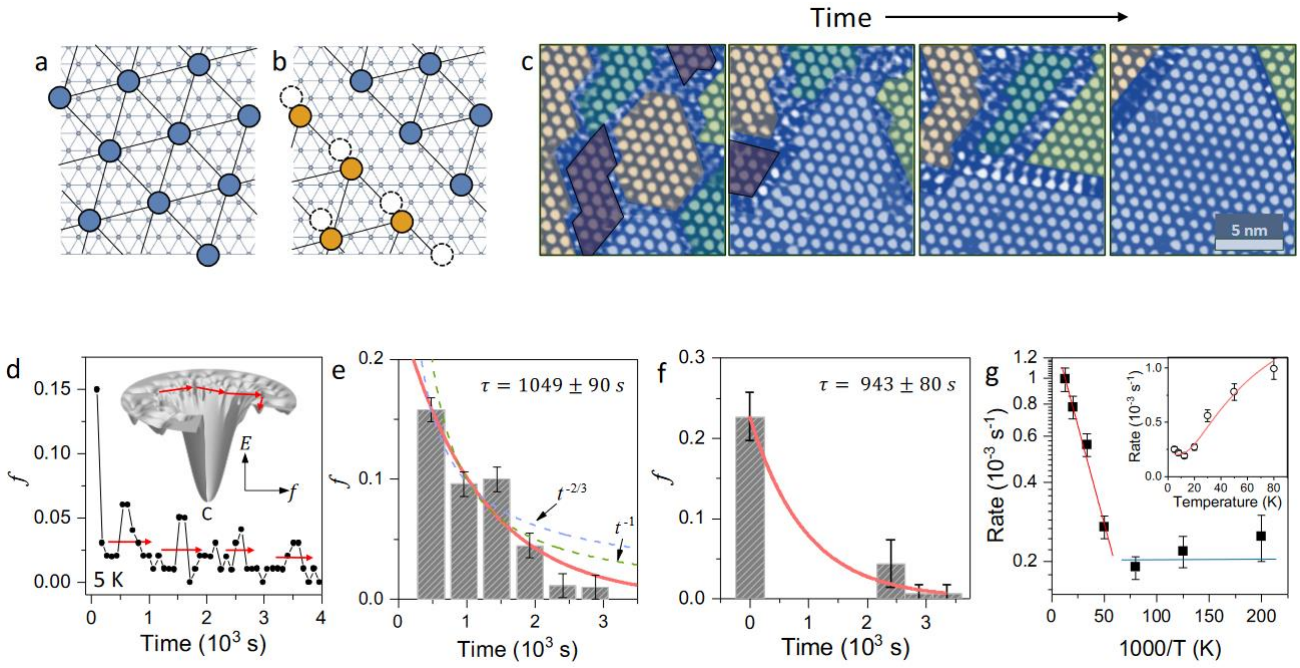

Figure 1. Domain reconfigurations in 1T-TaS_2. a) The crystal lattice showing Ta atoms (small circles). Occupied electron sites (blue and orange circles) **a**) in the ground state, and **b**) near a domain wall. **c**) A series of STM measurements at regular time intervals showing domain reconfiguration. Domains are colored to signify a displacement relative to the main commensurate lattice (light blue). (STM parameters: -0.8 V, 50 pA). **d**) The fraction of electrons moved $\boldsymbol{f(t)}$ as a function of time measured within the same area at $\mathbf{5}\,\boldsymbol{K}$. The jumps correspond to large (observable) configurational changes. The inset shows a schematic of the configurational free energy $\boldsymbol{E}$ as a function of configurational coordinate (Hamming distance) $\boldsymbol{f}$. The excited states within each well represent states which conserve $\boldsymbol{f}$ (see text). **e**) $\boldsymbol{f(t)}$ averaged over different areas of the sample, with periodic STM scans. Exponential and power law fits to the data are shown (solid and dashed lines respectively). Error bars represent counting errors. **f**) Same as **e**), except with a 32-minute gap in scanning the first point. The exponential fit is the red line. **g**) The temperature dependence of $\boldsymbol{R}$ averaged over a large number of decays on a logarithmic scale with the inset showing a linear scale.

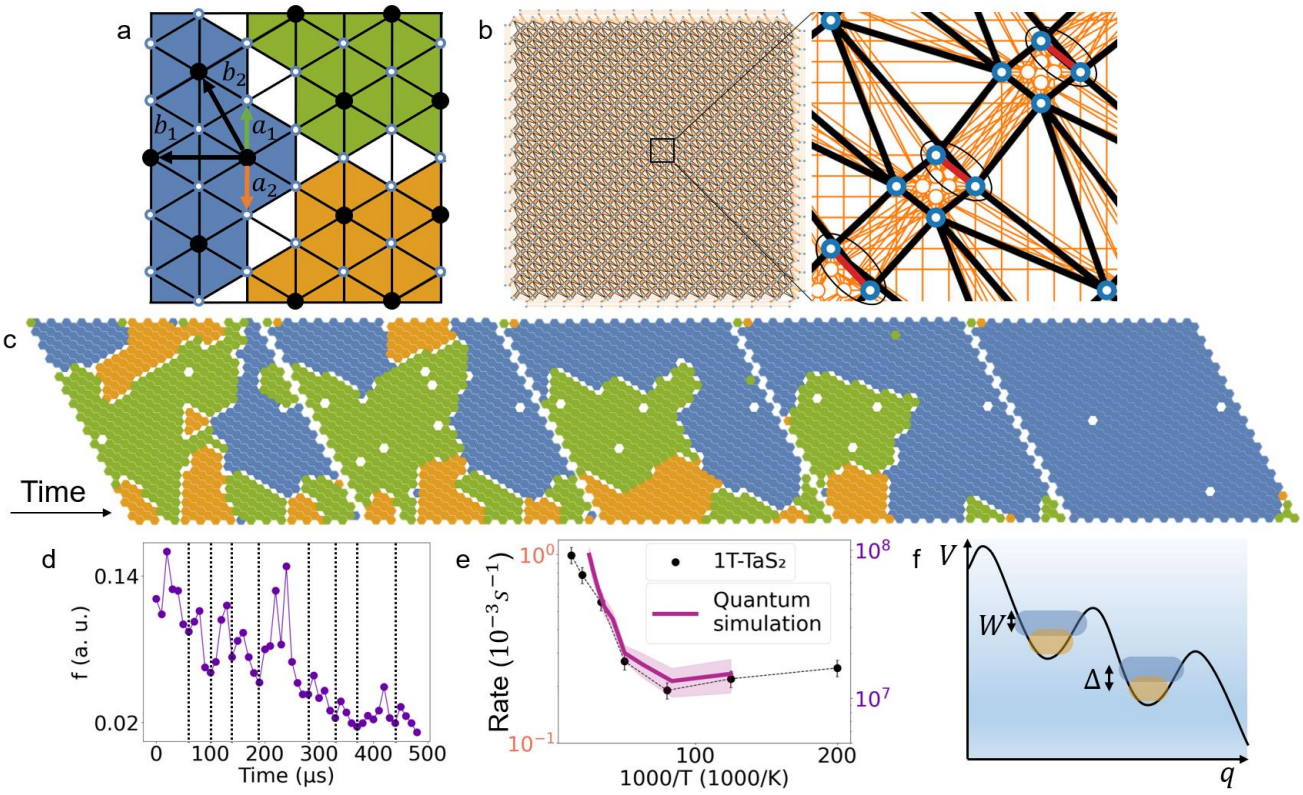

Figure 2. Simulation of emergent quantum decay based on microscopic quantum simulations. **a**) The three possible ground states of the NN repulsion we deployed on the quantum annealer. They are a $\mathbf{1/3}$ polaronic lattice with primitive vectors $\boldsymbol{b_1}$ and $\boldsymbol{b_2}$, shifted by two possible atomic lattice vectors $\boldsymbol{a_1}$ and $\boldsymbol{a_2}$. The different superlattices are colored for clarity. **b**) Embedding of the triangular lattice used in our simulations on the PQA with the inset showing the detailed connections between qubits. The white dots encircled with blue represent individual atomic sites (also in c)), black lines are connections between qubits we used for the nearest neighbor repulsion, red lines are physical connections used for creating logical qubits (also encircled in black) on a triangular lattice and the orange lines are the unused physical connections on the processor. **c)** An example of a relaxation sequence with parameters $\boldsymbol{t_a = 5\,\mu s}$, $\boldsymbol{r = 9}$ and $\boldsymbol{T_{eff} = 1.33}$. **d**) The Hamming distance $\boldsymbol{f(t)}$ sampled from the quantum annealer for the sequence shown in c). This can be compared with experimental data in Fig. 1d). Black dashed lines show the intermediate metastable states that emerge during the relaxation process. **e)** $\boldsymbol{R(T)}$ extracted from the PQA with parameters $\boldsymbol{t_a = 5\,\mu s}$ and $\boldsymbol{r = 15}$, and 1T-TaS_2. The temperature scale for the PQA was chosen to be $\boldsymbol{T = T_{eff} * 4K}$, for demonstration purposes. See SI for actual parameter estimation. **f**) The washboard potential of the PQA flux qubit with 2-level system spacing $\boldsymbol{\Delta}$ coupled to the external bath with an integral over noise $\boldsymbol{W}$.

Acknowledgments

We wish to acknowledge discussions with Tomaž Prosen, Marko Žnidarič, Andrew King and Tomaž Mertelj. Single crystals were grown for this work by Petra Sutar, funding from ARRS project P-0040, P2-0415, N1-0092 and young researcher grants, P17589 and P08333. This project has received funding from the European Union's Horizon 2020 research and innovation program under the Marie Skłodowska-Curie grant agreement No 701647.

Author Contributions

Michele Diego, Yevhenii Vaskivskyi, Yaroslav Gerasimenko and Dragan Mihailovic performed experimental measurements and analysis of experimental data. Jaka Vodeb conceptualized and performed quantum simulations on D-Wave's quantum annealer. Leonard Logaric and Viktor Kabanov performed theoretical analysis of data from experiment and simulation. Benjamin Lipovsek and Marko Topic performed simulations of Joule heating from the STM tip. Jaka Vodeb and Dragan Mihailovic wrote the paper. All authors contributed to the supplementary information.

Competing Interest Declaration

The authors declare no competing interests.

Supplementary Information

Supplementary Information is available for this paper.

Corresponding author

Correspondence and requests for materials should be addressed to Jaka Vodeb (jaka.vodeb@ijs.si).